Article

Stabilizing the Chemistry of NiO$_x$ in Perovskite Solar Cells to Pass the Damp Heat Test

Marion Dussouillez [1,2,*,†], Mounir Mensi [3], Ivan Marozau [1], Quentin Jeangros [1], Sylvain Nicolay [1,‡], Christophe Ballif [1,2] and Adriana Paracchino [1,*]

[1] CSEM Sustainable Energy Center, Rue Jaquet-Droz 1, 2002 Neuchâtel, Switzerland
[2] Laboratory of Photovoltaics and Thin Film Electronics, Institute of Electrical and Micro-Engineering (IEM), Ecole Polytechnique Fédérale de Lausanne (EPFL), Rue de la Maladière 71b, 2000 Neuchâtel, Switzerland
[3] X-Ray Diffraction and Surface Analytics Platform, Ecole Polytechnique Fédérale de Lausanne (EPFL), Rue de l'Industrie 17, 1951 Sion, Switzerland
* Correspondence: marion.dussouillez@gmail.com (M.D.); adriana.paracchino@csem.ch (A.P.)
† Current address: Solarlab Aiko Europe GmbH, Berliner Allee 29, 79110 Freiburg im Breisgau, Germany.
‡ Current address: Rolex S.A., David-Moning-Strasse 9, 2504 Biel, Switzerland.

Abstract: NiO$_x$ is widely used as a hole transport material in perovskite solar cells (PSCs). This wide band gap p-type material is conveniently deposited via high throughput RF-sputtering, making it suitable for the industrialization of PSCs. Nonetheless, for the cells to pass accelerated degradation tests such as the IEC 61215 damp heat (DH) test, the chemistry of the NiO$_x$ film should remain constant at elevated temperaturs to preserve its optoelectronic properties. This study emphasizes that structural defects resulting from Ni vacancies in NiO$_x$ lead to significant degradation of the PSCs after just a few hours of exposure to elevated temperatures (85 °C). We introduce here an approach to fine-tune the chemistry of the NiO$_x$ film by adjusting the gas flow during sputtering deposition and by incorporating Cs. Through this control on the chemistry of the layer, the optimized NiO$_x$-based PSCs exhibit remarkable stability, with devices passing 5 times the IEC 61215 norm (<5% rel after 5000 h of DH testing) and also showing better stability under light soaking. XPS analysis reveals that the concentration of Ni^{3+} in the bulk of the standard NiO$_x$ film is twice that in the optimized NiO$_x$. This suggests that the Ni^{3+} concentration, typically equal to the Ni vacancy concentration and beneficial for charge transport in NiO$_x$, may actually compromise the stability of the PSCs. Additionally, the film density of the optimized NiO$_x$ film was significantly higher than that of the standard film.

Keywords: doped-NiO$_x$; perovskite solar cell; stability; industrialization

1. Introduction

To continue the learning curve of silicon PV in the years to come, one of the most promising approaches is to fabricate a tandem device by adding a perovskite cell on top of a silicon one to increase efficiency. However, an important commercialization pre-requisite for such a technology is that it should at least pass the IEC 61215 standard degradation tests set up by the silicon industry, notably the damp heat (DH) test (85 °C, 85% relative humidity). Regarding the industrialization of these devices, NiO$_x$ seems to be one of the most promising hole transport materials (HTM). Indeed, this p-type inorganic material can be deposited by sputtering [1,2], a well-known industrial process. This high throughput technique allows the deposition of conformal layers compatible with flat [3] or textured [4–6] substrates.

Nevertheless, it has been previously demonstrated that NiO_x suffers from variations in oxidation state with time, and this reaction is accelerated when exposed to temperatures higher than room temperature in an inert atmosphere [7,8]. In solar cells, these changes lead to significant and irreversible degradation characterized by the emergence of an S-shape in the current-voltage (J-V) curve. This result is visible with NiO_x-based PSCs stored for a few months in N_2 box but also with encapsulated cells after only 100 h of DH. In the absence of oxygen in the environment, Ni vacancies, which determine the charge carrier concentration in the film, diffuse out and annihilate at the interfaces of the film [8], resulting in a decrease in the NiO_x conductivity. Moreover, Ni^{3+} species, which compensate for the Ni vacancies, may react with the iodide ions of the perovskite, lowering V_{OC} [9] and introducing instabilities [7]. To mitigate undesired redox reactions at the NiO_x/perovskite interface, Itzhak et al. proposed to protect the sputtered NiO_x surface with a thin Ni_yN layer sputtered from a Ni target in Ar and N_2 gas flows [10]. Peng et al. employed a thin layer of phenylethylamine iodide (PEAI) to reduce Ni^{3+} at the surface of sputtered NiO_x [11]. Other interlayers such as PN4N [12], 1,3-bis(diphenylphosphino)propane (DPPP) [13], 4-iodo-2,3,5,6-tetrafluorobenzoic acid (I-TFBA) [14] or 4′,4‴-(1,3,4-Oxadiazole-2,5-diyl)bis(N,N-bis(4-methoxyphenyl)-[1,1′-biphenyl]-4-amine) [15] have been proposed to passivate the defects at the NiO_x/perovskite interface, leading to an improvement in the reliability of the devices. The use of self-assembling monolayers on the NiO_x can also decrease the trap states density at the NiO_x/perovskite interface, resulting in a better charge extraction thanks to a better band alignment [16–18]. We have previously shown that reducing the thickness of the NiO_x layer down to 5 nm and adding an organic layer on its top surface such as a self-assembling monolayer (e.g., MeO-2PACz) helps mitigating fill factor (*FF*) losses during DH testing [7]. This study demonstrated that, under thermal stress, the NiO_x doping concentration drops by 3 orders of magnitude, and its valence band shifts downwards, creating a band alignment mismatch with the valence band level of the perovskite [7]. With aging in an oxygen-free environment, NiO_x loses Ni^{3+}, leading to an increase in the thermally more stable Ni^{2+} [8,19]. This irreversible change leads to the formation of a strong hole extraction barrier.

To address this issue, the NiO_x chemistry must remain constant, also at the elevated temperatures reached during damp heat testing. Several research papers have explored the enhancement of the NiO_x conductivity by introducing various dopants into the film, such as Al [20], Cs [21], Mg [22], Na_2S [23], Li [24,25], and O [26]. We present a method to modify the chemistry of the NiO_x film by adjusting the gas flow during the sputtering deposition process and incorporating cesium and we examine the performance and stability of cesium-doped NiO_x under elevated temperatures pertinent to damp heat testing. By incorporating Cs, the formation of a Ni^{3+} ion is expected for every Cs^+ that substitutes a Ni^{2+}. With this approach, we demonstrate an improved thermal stability in DH conditions (85 °C, 85% relative humidity), with PSCs remaining stable for more than 5000 h. Additionally, adjusting the NiO_x chemistry also improves the light soaking stability of NiO_x-based PSCs, with a champion cell showing no performance loss after more than 1200 h under 1 sun at 25 °C in N_2 (+0.5% efficiency relative to the initial value at the end of the test).

2. Materials and Methods

2.1. Materials

FAI and FABr (99.99%) were purchased from Dyenamo (Stockholm, Sweden), PbI_2 (99.99%), $PbBr_2$ (99.99%) and MeO-2PACz (>98.0%) from TCI Europe N.V. (Zwijndrecht, Belgium), CsI (99.99%) from Alfa Aesar (Kandel, Germany), and C_{60} from Creaphys (Dresden, Germany). All the other chemicals were bought from Sigma-Aldrich (Buchs SG, Switzerland).

2.2. Solar Cell Fabrication

P-i-n single junction perovskite solar cells were fabricated on commercial 2.5 cm × 2.5 cm glass/ITO substrates from Kintec, featuring a sheet resistance of 7 Ω/sq. For substrate cleaning, glass substrates are loaded into commercial plastic racks and subsequently washed in a Miele PG8536 industrial cleaner. The cleaning process consists of several steps. The first step is deionized (DI) water rinsing, followed by an alkaline clean using Deconex 20 NS-x detergent, a second DI water rinse, a neutralization with Deconex 20 Organacid acidic cleaner and neutralizer, and a final DI water rinse.

For the HTM, 20 nm of NiO_x or $Cs:NiO_x$ were RF sputtered from a NiO_x or $Ni_{0.99}Cs_{0.01}O_x$ target from Disc AG. The diameter of the targets was 100 mm. These sputtering processes were conducted in an Oerlikon Clusterline cluster tool following an oxygen plasma cleaning on the ITO in a RIE chamber (with parameters: 250 W, 50 sccm O_2 flow, working pressure 100 mTorr for 60 s). Both NiO_x and $Cs:NiO_x$ were sputtered at 150 W, with varying gas flows: either in pure Ar (150 sccm) or in Ar/O_2 atmosphere (120 sccm Ar/30 sccm $Ar_{0.95}$-$O_{2(0.05)}$). The chuck

temperature was maintained at 60 °C. Just before fabricating the devices, NiO_x and $Cs:NiO_x$ films were annealed at 300 °C for 30 min in an air environment. For some devices, a 100 uL MeO-2PACz solution was prepared and spin-coated in a nitrogen-filled glovebox on top on the NiO_x films (1 mM in ethanol, 3000 rpm for 30 s, static spin-coating). The films were subsequently dried in a glovebox at 100 °C for 10 min. The double cation $Cs_{0.17}FA_{0.83}Pb(I_{0.83}Br_{0.17})_3$ perovskite solution was prepared in a glovebox by mixing three solutions in the ratio 17:66:17. First solution: PbI_2 (1.5 M) and CsI (1.22 M) dissolved in DMSO at 70 °C. Second solution: PbI_2 (1.5 M) and FAI (1.22 M) in DMF:DMSO (4:1 as a volume ratio) at 70 °C. Third solution: $PbBr_2$ (1.5 M), FABr (1.01 M) and CsBr (0.207 M) dissolved in DMSO. 100 μL of this prepared perovskite solution was then spin coated using a 2 steps program: 10 s at 1000 rpm, then 37 s at 6000 rpm. 300 μL of ethyl acetate was quickly dripped on the sample 5 s before the end of the program. Films were first dried for 2 min at 60 °C, and then annealed for 30 min at 120 °C in the glovebox. For light soaking degradation test, a $Cs_{0.04}FA_{0.72}MA_{0.24}Pb(I_{0.75}Br_{0.25})_3$ perovskite solution approaching stoichiometric conditions (0.7% PbI_2 excess) was used. The "stoichiometric" perovskite solution was prepared by mixing three stock solutions with 830:170:40 volume ratio. For the first solution, 1.36 M FAI and 1.43 M PbI_2 were dissolved in 4:1 (volume ratio) DMF:DMSO. For the second solution, 1.36 M MABr and 1.43 M $PbBr_2$ were dissolved in 4:1 DMF:DMSO. For the third solution, 1.5 M CsI was dissolved in DMSO. 100 μL of this prepared perovskite solution was then spin coated using a 1 step program: 35 s at 3500 rpm. 300 μL of anisole was quickly dripped on the sample 10 s before the end of the program. Perovskite films were annealed for 20 min at 100 °C in a N_2 glovebox. For the electron transport layer, LiF (1 nm) and of C_{60} (20 nm) were thermally evaporated in an Angstrom evaporator (400 °C, 0.1 Å/s and 700 °C 0.2 Å/s respectively). A 10 nm SnO_2 layer was then deposited by ALD in an Oxford Instruments FlexAL ALD system (at 100 °C, using water and Tetrakis(dimethylamino)tin(IV) (99.99%-Sn, Strem Chemicals) as precursors). 110 nm of ITO was sputtered in a Oerlikon Clusterline cluster tool (at 750 W, under 25/8 sccm of $Ar/Ar-O_2$ flow, and a shuck at 80 °C). A 120 nm thick silver electrode was evaporated using a custom-built evaporator at a rate of 0.3–1 Å/s. For DH testing, the completed PSCs were encapsulated in between two 5×5 cm^2 glasses, including a polyolefin lamination foil, seal with a butyl edge sealant. Adhesive conductive ribbons were employed to connect the encapsulated cells. The complete stack was then laminated in a 3S laminator at 120 °C with a maximum pressure of 0.6 bar.

2.3. Device Characterization

The current density-voltage (J-V) curves of the solar cells were measured with a Wacom two-lamp (Ha and Xe) AAA class sun simulator with a AM1.5 G spectrum at 1000 W/m^2. The active area of the solar cell was defined by a metal mask with an aperture area 1.04 cm^2. The cells were measured from -0.2 V to 1.2 V and from 1.2 V to -0.2 V with a scan rate of 100 mV/s using an integration time of 0.1 s and a delay of 0.1 s for each data point, and the voltage step was 0.02 V. The external quantum efficiency (EQE) of the cells was measured using a custom-made setup using a lock-in amplifier, a chopped white light source (900 W, halogen lamp, 260 Hz) and a dual grating monochromator.

2.4. Film Characterization

The total transmittance and total reflectance spectra of the films, from which the absorptance spectra were obtained, were measured with a PerkinElmer Lambda 950 UV-VIS-NIR spectrophotometer equipped with an integrating sphere. Film thickness was measured using a KLA-Tencor P-15 Profiler or by ellipsometry (J. A. Woollam Co.).

The XRD patterns were measured in the Bragg–Brentano geometry with a PANalytical X'Pert PRO diffractometer (Cu Kα radiation, wavelength 1.54 Å), in the 2theta range of 10–90° with a step of 0.013°. For XRR and GI-XRD measurements we used a Panalytical X'Pert MRD diffractometer equipped with a parallel beam mirror and a point detector. For the GIXRD experiment we used a grazing incident angle of 0.3°. For the XRR measurement the incident beam slit was set to 1/32° and a 0.04 rad Soller slit was used at the detector side to minimize the divergence of the X-ray beam. The measurements were performed in the 2theta range of 5–90°. For both GIXRD and XRR measurements we used 100 nm-thick films on glass (GIXRD) and on Si wafer (XRR). The data fitting was done using the X'Pert Reflectivity software.

STEM bright-field images and energy-dispersive spectra of the different NiO_x films with and without Cs were acquired using a FEI Osiris microscope operated 200 kV. The samples were prepared by sputtering the NiO_x films directly on electron transparent SiN windows.

High-resolution XPS analysis was conducted using an Axis Supra (Kratos Analytical) XPS equipped with a monochromatic Al Kα X-ray source. The pass energy was adjusted to 20 eV with a step size of 0.1 eV. To minimize charging effects, the samples were electrically grounded. Sample etching was performed using an Ar ion beam. The

Ni oxidation states were determined by fitting components corresponding to the electronic states of Ni^0 (from Ni metal), Ni^{2+} (from the cubic rock-salt structure NiO), and Ni^{3+} (from NiOOH), as described by Biesinger et al. [27,28].

Damp heat degradation test on glass-glass laminated cells were run in a Weiss Technik weathering chamber set at 85 °C and 85% relative humidity.

3. Results and Discussion

For the PSCs, the solar cell stack is shown in Figure 1a with NiO$_x$ films (20 nm) as hole transport layer. The finished devices were encapsulated between 2 glasses, with a thermoplastic lamination foil on both sides and a butyl rubber edge sealant to protect from moisture ingress.
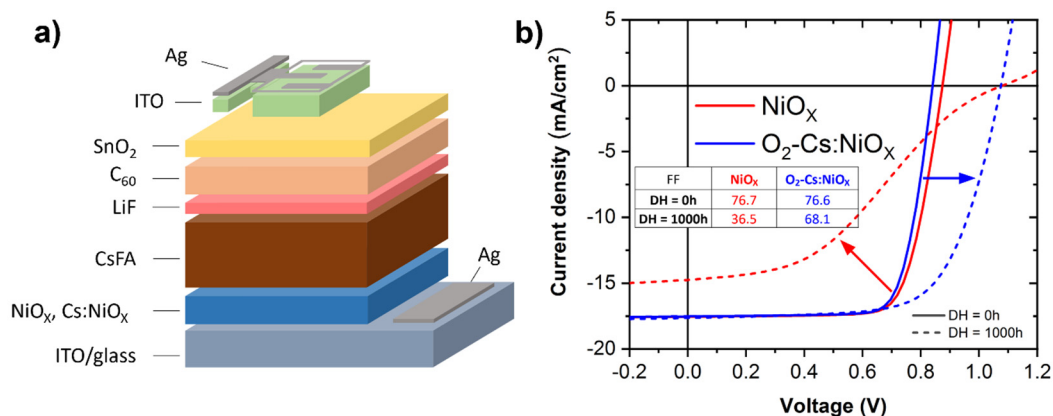

Figure 1. Solar cell architecture and performance comparison for NiO$_x$ and O$_2$-Cs:NiO$_x$ HTMs. (**a**) device architecture, (**b**) J-V curves of encapsulated PSCs before and after damp heat: the red and blue curves correspond to NiO$_x$ and O$_2$-Cs:NiO$_x$, respectively.

As explained earlier, the NiO$_x$ film chemistry should be stabilized such that its conductivity and valence band do not shift during aging. Ni^{3+} species are required to ensure a good hole conductivity. These Ni^{3+} species, arising from the loss of an additional electron compared to Ni^{2+} and preserving overall charge neutrality thanks to Ni vacancies, introduce a mobile hole in the NiO$_x$ valence band [29]. However, Ni^{3+} tend to react with iodide from the perovskite through the following redox reaction: $2Ni^{3+} + 2I^- \rightarrow 2Ni^{2+} + I_{2(g)}$ [7,9,11]. While the standard NiO$_x$ (named NiO$_x$ hereafter) was sputtered in pure Ar (150 sccm), for the optimised NiO$_x$ we sputtered NiO$_x$ from the same target but with an Ar/O$_2$ gas mixture to increase the oxygen-to-nickel ratio in NiO$_x$, for which we expected a higher doping [8,19,26,30]. In order to increase the Ni^{3+} concentration further, and thus enhance the hole conductivity, NiO$_x$ was also doped with Cs by sputtering a Ni$_{0.99}$Cs$_{0.01}$O$_x$ target under an Ar/O$_2$ gas flow mixture. Hereafter, the NiO$_x$ and Cs:NiO$_X$ sputtered with an oxygen partial pressure 120 sccm Ar/30 sccm Ar$_{(0.95)}$-O$_{2(0.05)}$ are named O$_2$-NiO$_x$ and O$_2$-Cs:NiO$_x$, respectively. They were all sputtered in the same chamber, at the same power (150 W, target diameter 100 mm). In terms of optical properties, the as-deposited O$_2$-NiO$_x$ and O$_2$-Cs:NiO$_x$ films appear significantly less transparent compared to NiO$_x$, but after the post-annealing at 300 °C the films become similarly transparent (Figure S1). This difference in the as-deposited films arises from sputtering under O$_2$ gas, which increases the relative oxygen-to-nickel ratio and consequently elevates the concentration of Ni^{3+} [9], darkening the film [31]. After annealing at 300 °C in air, the three films become similarly transparent, suggesting the release of excess oxygen and the annihilation of Ni^{3+} states. This observation on the optical properties is confirmed from the chemical analysis provided in Section 3.4. In other words, although we increased the oxygen content and sputtered from a Cs-doped NiO target with the idea of increasing the doping, our post-annealing in air removed the excess oxygen present in the films. Nevertheless, the fact of using oxygen during the sputtering clearly impacted the film properties, as it will be detailed in Section 3.3, and changed the device performance as it will be presented in the following section.

3.1. Devices Performances—NiO$_x$

In semi-transparent devices, O$_2$-Cs:NiO$_x$-based PSCs exhibit statistically lower efficiencies (12% on average, versus 12.6% for NiO$_x$) mainly due to a lower V_{OC} (−50 mV on average, Figures 1b and S2a,d), attributed to a less oxidized surface with lower Ni^{3+} content (as shown later in the XPS results). Photoluminescence (PL) data in Figure S3 supports this result, indicating higher non-radiative recombination in O$_2$-Cs:NiO$_x$ devices. *FF* and J_{SC} are similar between the different NiO$_x$ films (Figures 1b and S2b,c). Despite lower initial performances, O$_2$-Cs:NiO$_x$-

based devices gain in efficiency compared to NiO_x-based PSCs after 1000 h of DH testing (Figures 1b and S4). For both types of cells, the V_{OC} increases rapidly in the first hours of DH testing. This result is consistent with PL measurements after thermal aging, showing reduced non-radiative recombination for both films (Figure S3). However, while the *FF* of NiO_x cells drops systematically to <50% within the first 100 h of testing, the *FF* of O_2-Cs:NiO_x-based cells decreases by about 10% after 1000 h (Figure S4).

3.2. Devices Performances—NiO$_x$/SAM

As discussed in our previous publication [7], the presence of an organic HTM (self-assembling monolayer or polymer) at the interface between NiO and perovskite alleviates the formation of an S-shape in the J-V curves of cells exposed to DH conditions. Thus, cells combining either NiO_x, O_2-NiO_x or O_2-Cs:NiO_x with a MeO-2PACz self-assembled monolayer (SAM) were exposed to DH conditions. Figures 2, S5 and S6 present the J-V curves and J-V parameters obtained for each HTM stack after different DH testing durations.

Initially, fresh devices showed similar *FF* values, with a slight dispersion possibly due to imperfect SAM coverage (Figure S5a). After 160 h of DH testing, all devices showed an increase in V_{OC} as seen in Figure 2a–c (light-blue curves). However, after 1000 h of test, the *FF* of NiO_x-based devices dropped to 60%, accompanied by a visible increase in series resistance (R_{OC}) in J-V data, from 7.5 $\Omega\cdot cm^2$ to 17.5 $\Omega\cdot cm^2$ (Figures 2d and S5b). In contrast, O_2-NiO_x and O_2-Cs:NiO_x devices remained much more stable, with a R_{OC} below 8 $\Omega\cdot cm^2$.

After 2000 h, the degradation of NiO_x devices became even more pronounced, with the *FF* dropping below 55% (Figure S5c) and a strong increase in R_{OC} (Figure 2d). Conversely, O_2-NiO_x and O_2-Cs:NiO_x PSCs maintained *FF* values above 70% and 73%, respectively.

After more than 5100 h of DH testing, thus 5 times the IEC 61215 standard, the best J-V scan of O_2-Cs:NiO_x device exhibited a *FF* of 73.5% and an efficiency of 13.7% (Figure 2c,e,f), whereas O_2-NiO_x cells showed a decreased *FF* to 67.1% and an efficiency of 12.6% for the best J-V scan (Figures 2b,d and S6). This discrepancy is attributed to the increased series resistance in O_2-NiO_x-based devices, which reached 11.9 $\Omega.cm^2$, compared to 7.6 $\Omega.cm^2$ for O_2-Cs:NiO_x-based device (Figure 2d), with the latter remaining stable in performance throughout the 5100 h of testing.

Additionally, while an increase in V_{OC} was observed during the first hours of DH testing across all NiO_x conditions (Figures 2 and S6) [32], a sharp decrease in J_{SC} was observed only for the NiO_x-based device, accompanied by the appearance of a bright yellow regions within its active area after 5100 h of DH testing (Figure S6e). This significant degradation is particularly evident on the substrate side of the device (i.e., the NiO_x side), suggesting that substantial degradation is initiated at the perovskite/NiO_x interface [9]. This reaction is notably less pronounced in O_2-Cs:NiO_x and O_2-NiO_x cells, which is consistent with the J-V data.
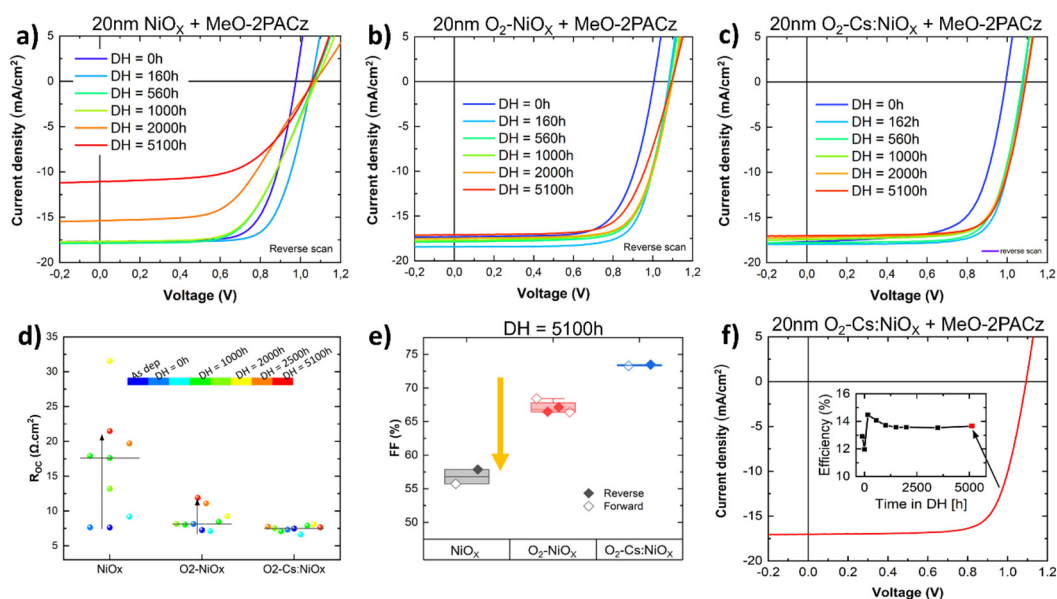

Figure 2. >5000 h of DH stability with using O_2-Cs:NiO_x/MeO-2PACz as HTM. (**a**) reverse J-V curves of semi-transparent PSCs based on NiO_x/MeO-2PACz, (**b**) O_2-NiO_x/MeO-2PACz, and (**c**) O_2-Cs:NiO_x/MeO-2PACz, during 5100 h of damp heat testing. DH = 0 h corresponds to the J-V measurement after encapsulation and thus, just before the beginning of the test, while DH = 5100 h corresponds to the J-V measurements of the cells after

more than 5100 h (7 months) in the DH chamber (85 °C, 85% R. H.); (**d**) Series resistance (R_{OC}) and (**e**) FF of these cells as a function of DH testing; and (**f**) reverse J-V curve of the record cell based on O_2-Cs:NiO_x/MeO-2PACz after enduring 5100 h of test. The active area of the cells is 1 cm^2.

By modifying the NiO_x film chemistry the degradation occurring at the NiO_x/perovskite interface can be effectively mitigated. Preliminary light soaking tests were also performed on semi-transparent PSCs using both NiO_x and O_2-NiO_x, confirming the higher stability of the latter. The variation in J-V parameters over time under light exposure at 35 °C under 1-sun conditions are shown in Figure S7. While the NiO_x devices showed a 20% relative efficiency loss after 1200 h of light soaking, the O_2-NiO_x devices had no degradation. Overall, these preliminary light soaking results point in the direction of our damp heat findings and emphasize the importance of controlling NiO_x stoichiometry to enhance PSC stability.

Given the strong differences in device stability, advanced characterization techniques such as atomic force microscopy (AFM), scanning transmission electron microscopy (STEM), grazing incidence X-ray diffraction (GI-XRD) and X-ray photoelectron spectroscopy (XPS) were conducted on NiO_x, O_2-NiO_x and O_2-Cs:NiO_x films. Results are discussed below.

3.3. Film Characterization

To get some insights into the possible differences in the crystallinity of the O_2-Cs:NiO_x and the reference NiO_x films, STEM and GIXRD analyses were performed. The XRD patterns (Figure 3a) show that NiO_x crystallites are randomly oriented, with lower intensity peaks for O_2-Cs:NiO_x, indicating poorer crystallinity due to Cs addition. The shift in XRD peaks to lower 2θ angles for O_2-Cs:NiO_x sample (Figure 3a) suggests lattice expansion, consistent with the incorporation of the large Cs into the NiO_x lattice (Cs^+ radius of 1.67 Å, compared to 0.55 Å for Ni^{2+}) [33]. Energy-dispersive X-ray spectroscopy (EDX) confirmed the presence of about 0.5%at of Cs in the film (Figure S8). Despite small lattice distortion, both NiO_x and O_2-Cs:NiO_x films show similar morphology in STEM bright-field images (Figure S9). X-ray reflectivity (XRR) data revealed a density of 5.6 g/cm^3 for O_2-NiO_x on silicon, against 4.9 g/cm^3 for NiO_x, indicating that O_2-NiO_x is denser. Atomic force microscopy (AFM) highlighted a roughness of 2.6 nm for the O_2-NiO_x film on silicon while the NiO_x film appeared twice rougher (5.0 nm), as shown in Figures 3b,c and S10. Consequently, the film growth in the presence of oxygen, which proceeded at a rate five times slower than in pure Ar, led to smoother and denser films. As the sputtering of the O_2-Cs:NiO_x was done in the same conditions as for O_2-NiO_x (same gas flow and similar deposition rates), a denser and smoother layer is also expected for O_2-Cs:NiO_x compared to NiO_x. As an indication, the deposition of a 20-nm film of NiO_x took 5 min, whereas 25 min were required for O_2-NiO_x and O_2-Cs:NiO_x.
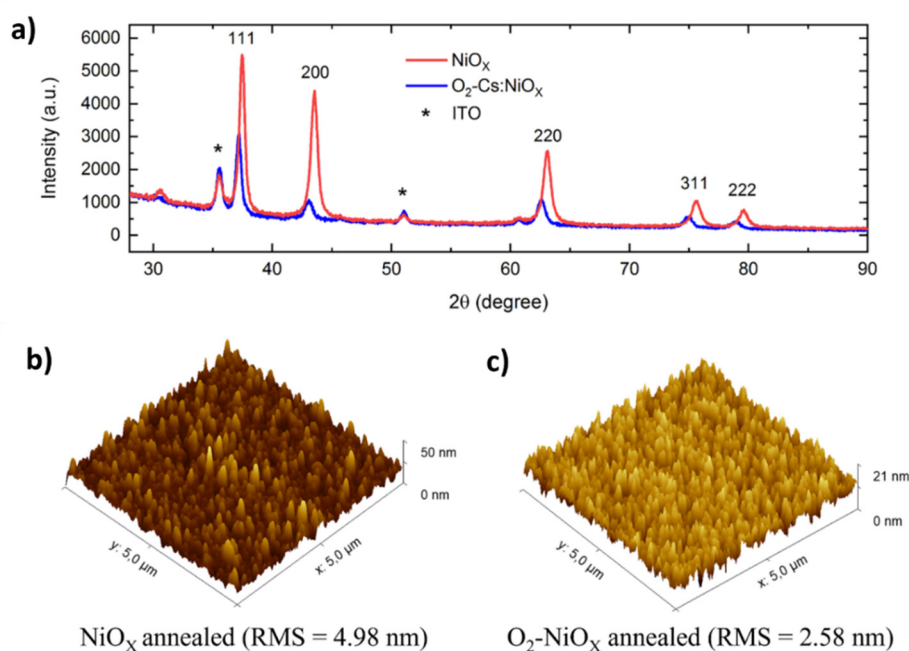

Figure 3. Characterization of NiO_x and O_2-Cs:NiO_x Thin Films and Their Microstructures. (**a**) Grazing incidence measurement (0.3°) of 100 nm thick NiO_x (red) and O_2-Cs:NiO_x (black) film on ITO substrate, (**b**) AFM images of both annealed NiO_x and (**c**) O_2-NiO_x deposited on glass/ITO substrates.

3.4. Chemical Analysis of the Different NiO Films

To understand the surface chemistry of NiO_x, O_2-NiO_x and O_2-Cs:NiO_x films, X-ray photoelectron spectroscopy (XPS) was performed on fresh and "thermally aged" films, which were annealed in nitrogen at 85 °C for one week to simulate damp heat conditions with an impermeable encapsulation (Figure 4). XPS depth profiling was also conducted to analyze the evolution of the $Ni2p_{3/2}$ signal from the surface of the various NiO films down to the ITO interface and to compare the Ni^{3+} amount between samples (Figure 5).

Using the approach described by Biesinger et al. [27], the $Ni2p_{3/2}$ peaks were deconvoluted to evaluate the amount of Ni metal, oxide, oxy-hydroxides, and hydroxide. XPS data acquired from the surface of the fresh and aged nickel oxide films is shown in Figures 4 a,c,e, S11 and S12. Only for NiO_x film, a distinct metallic Ni signal is present in the fresh sample but disappears in the aged sample (Figures 4 and S11). Moreover, the Ni^{3+} to Ni^{2+} ratio decreases upon aging at 85 °C. For O_2-NiO_x and O_2-Cs:NiO_x films, an opposite trend is observed: the concentration of Ni^{2+} decreases, while the Ni^{3+} content increases with aging. In addition, the fresh NiO_x surface shows nearly double the Ni^{3+} content (40%) compared to the surfaces of the O_2-NiO_x and O_2-Cs:NiO_x films (21–23%, Figure S11). This higher concentration could negatively impact performance and stability by oxidizing halides at the interface [9,11,29].
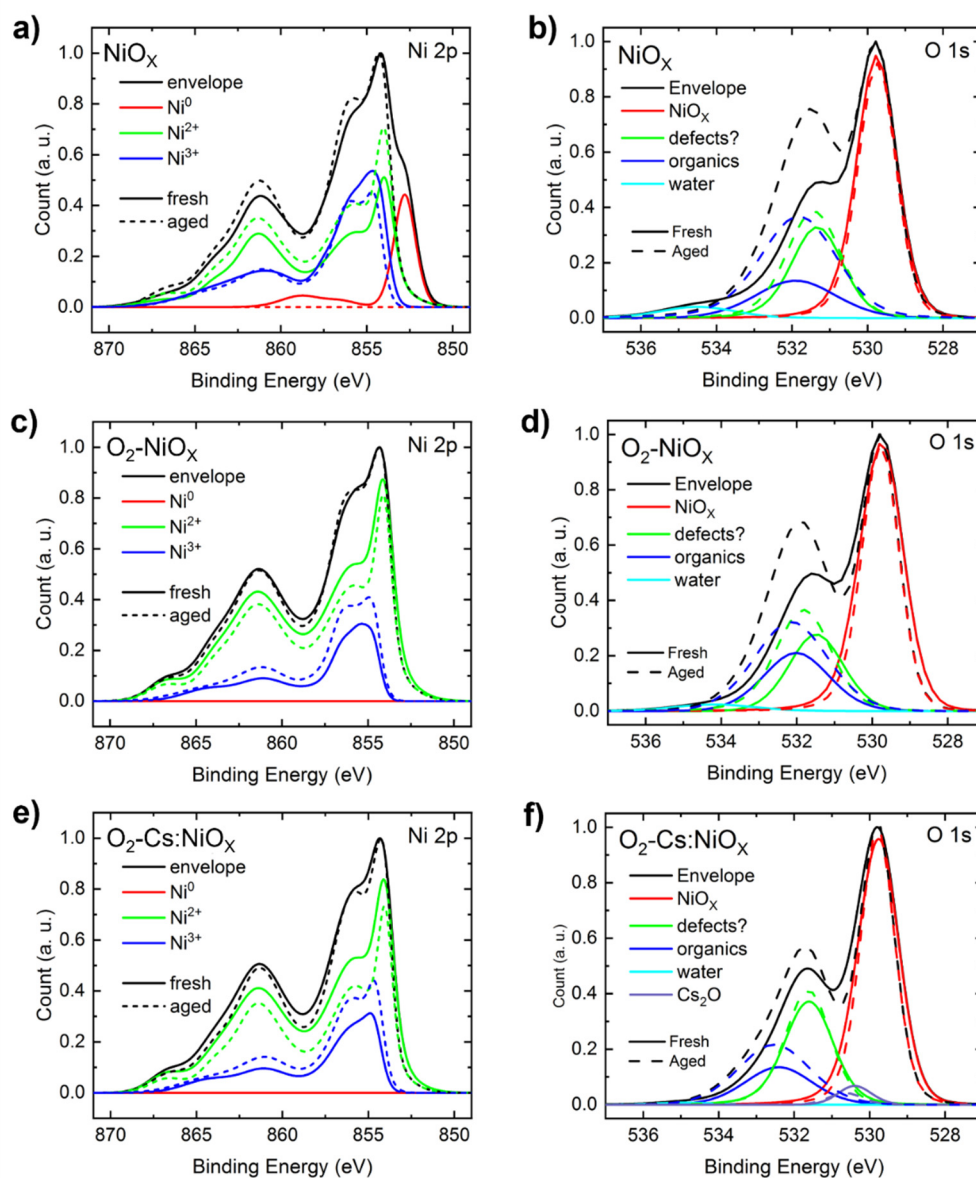

Figure 4. XPS measurements on fresh and aged films of NiO_x (**a,b**), O_2-NiO_x (**c,d**) and O_2-Cs:NiO_x (**e,f**). For each sample, the global Ni 2p or O 1s envelopes and their deconvolutions are plotted on the same graph.

More differences before and after aging are noticeable in the O1s peak (Figures 4b,d,f and S12). The O1s peak analysis reveals two distinct peaks, with the higher binding energy peak showing variations after aging,

particularly for NiO$_x$ and O$_2$-NiO$_x$. The deconvolution of this peak reveals four components: organic contamination, adsorbed water, a minor contribution of the oxygen from Cs$_2$O in the Cs:NiO$_x$ sample, and a remaining contribution at around 531.4 eV. This contribution can be assigned neither to NiOOH (the Ni:O ratio does not match) nor to Ni$_2$O$_3$ (the energy would rather be 531.7–531.8 eV) [34]. Instead, it could correspond to oxygen-containing species adsorbed at defects, most likely close to nickel vacancies (and therefore called defects in the figures), as reported by Biesinger [27,35].

The defect concentration, associated to the O defects peak, is larger in fresh NiO$_x$ (see graphs and table in Figure S12), with noticeable shifts towards higher energies in aged NiO$_x$ and O$_2$-NiO$_x$, but not for O$_2$-Cs:NiO$_x$ (see Figure 4b,d,f, green curves). This observation suggests that the incorporation of Cs into the lattice restricts chemical changes, resulting in a more stable layer upon annealing/aging. NiO$_x$ films also show more carbon contamination (organic contribution) after aging (Figure 4b,d,f, dark blue curves), likely due to its lower density/increased porosity resulting from the fast sputtering in pure Ar.

Depth-profiling XPS data reveals a higher concentration of Ni^{3+} in NiO$_x$ films compared to doped films (Figure 5). NiO$_x$ exhibited an uneven Ni^{3+} distribution that became uniform after aging, indicating that Ni vacancies migrate to the surface. In contrast, O$_2$-NiO$_x$ films showed a lower and consistent Ni^{3+} concentration throughout the bulk, with no changes after aging, suggesting that excess oxygen is eliminated during post-deposition annealing. O$_2$-Cs:NiO$_x$ films exhibit the fewest Ni^{3+}, possibly indicating that Cs$^+$ occupies V$_{Ni}$ sites rather than Ni^{2+} sites, thus reducing Ni^{3+} in the film. Despite similar film thicknesses, XPS depth profiling required more etching steps to reach the ITO interface for O$_2$-Cs:NiO$_x$ (see Figure 5, NiO$_x$ and O$_2$-NiO$_x$ could be etched 3 times faster than O$_2$-Cs:NiO$_x$ film), suggesting that the density of the film is higher. This finding supports the AFM and XRR results, which demonstrate a lower density for the NiO$_x$ film, and a greater propensity to adsorb water and organic contaminants.
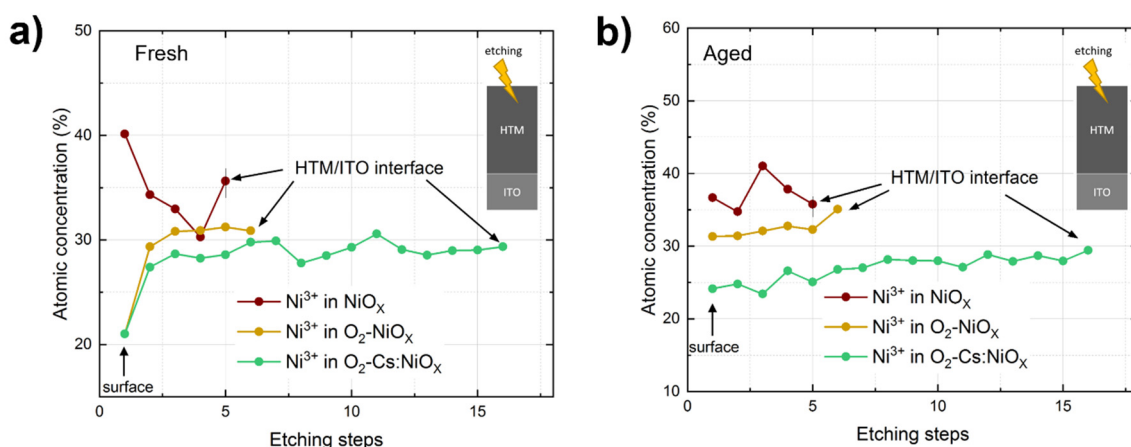

Figure 5. Ni^{3+} concentration as a function of depth in NiO$_x$, O$_2$-NiO$_X$ and O$_2$-Cs:NiO$_x$ films. (**a**) Fresh films after an annealing at 300 °C for 30 minutes, as in devices. (**b**) Films after 1 week aging in nitrogen at 85 °C, to simulate the effect of damp heat test with an impermeable encapsulation. The atomic concentration of Ni^{3+} species obtained from XPS depth-profile analysis for fresh and aged NiO$_x$, O$_2$-NiO$_x$ and O$_2$-Cs:NiO$_x$ films deposited on glass/ITO substrates. Aged samples were placed in an inert atmosphere at 85 °C for one week (same temperature as in the DH test). XPS measurements were conducted on the film surface and after each etching step to reveal the bulk composition. Identical etching parameters were applied to all samples, but the thickness removed by each etching step varied due to differences in film density of the NiO$_x$, O$_2$-NiO$_x$ and O$_2$-Cs:NiO$_x$ films. The XPS depth profiling was stopped at the ITO interface, which was identified by the detection of Sn peaks, with the interface position defined as Ni/Sn = 50%. While only 5 etching steps were required to reach the ITO surface in the case of NiO$_x$ samples, the O$_2$-Cs:NiO$_x$ demanded 16 steps, underscoring the lower density of NiO$_x$ compared to O$_2$-Cs:NiO$_x$.

Overall, these results underscore the chemical stabilization effect of sputtering in presence of O$_2$ and adding Cs in NiO$_x$, which translates into improved DH stability.

4. Conclusions

In summary, this study revealed that the NiO_x film sputtered in pure argon atmosphere is defective, quite porous and contains a large amount of Ni^{3+} at its surface. Consequently, the film becomes more susceptible to water adsorption, contamination, and prone to oxidize the perovskite absorber. A careful control of oxygen during NiO_x sputtering not only stabilizes the NiO_x film but also increases its density and makes it smoother, leading to better heat stability. Furthermore, the incorporation of a Cs element reduces the concentration of Ni^{3+} species, especially at the film surface, and restricted chemical changes under prolonged exposure to heat in an inert environment. As a result, PSC employing such O_2-Cs:NiO_x films remained stable for more than 5000 h of damp heat testing. These findings provide strategies for enhancing the long-term stability of perovskite solar cells featuring a hole transport material that can be manufacturing industrially.

Supplementary Materials

The following supporting information can be downloaded at: URL, Figure S1: Absorptance spectra of NiO_x, O_2-NiO_x and O_2-Cs:NiO_x; Figure S2: J-V parameters of as-deposited PSCs for NiO_x and O_2-Cs:NiO_x; Figure S3: Photoluminescence spectra of NiO_x/perovskite (red) and O_2-Cs:NiO_x/perovskite (blue) films coated on glass/ITO substrates; Figure S4: J-V performances of 1 cm^2 semi-transparent PSCs based on 20 nm NiO_x and O_2-Cs:NiO_x at different times of DH testing; Figure S5: FF of NiO_x/MeO-2PACz-based PSCs presented in Figure 2 during damp heat testing; Figure S6: J-V parameters of NiO_x/MeO-2PACz-based PSCs presented in Figure 2 as a function of DH aging; Figure S7: J-V parameters of PSCs based on NiO_x and O_2-NiO_x during light soaking at 35 °C and open-circuit conditions; Figure S8: Atomic concentration of Ni, O, and Cs determined by STEM EDX for NiO_x and O_2-Cs:NiO_x 20 nm films; Figure S9: Microstructure of NiO_x and O_2-Cs:NiO_x thin films; Figure S10: AFM images of both annealed NiO_x (left) and O_2-NiO_x (right) films; Figure S11: Ni 2p XPS surface analysis and deconvolution for each Ni oxidation state (Ni0, Ni^{2+} and Ni^{3+}) for NiO_x, O_2-NiO_x and O_2-Cs:NiO_x films; Figure S12: XPS analysis of O 1s spectra for NiO_x, O_2-NiO_x, and O_2-Cs:NiO_x surfaces before and after aging at 85 °C.

Author Contributions

M.D. and A.P. designed the experiments. M.D., M.M., I.M. and Q.J. performed the experiments and, with the help of A.P., analyzed the data. M.D. made the devices. M.M., I.M. and Q.J. provided support with respect to sample characterization. A.P., Q.J., S.N. and C.B. supervised different parts of the work. M.D. wrote the manuscript with support from all co-authors. All authors have read and agreed to the published version of the manuscript.

Funding

Data Availability Statement

The datasets generated during and/or analyzed during the current study are available from the corresponding author upon reasonable request.

Acknowledgments

Conflicts of Interest

The authors declare no conflict of interest.

References

1.   Cui, J.; Meng, F.; Zhang, H.; et al. CH3NH3PbI3-Based Planar Solar Cells with Magnetron-Sputtered Nickel Oxide. *ACS Appl. Mater.s Interfaces* **2014**, *6*, 22862.

2.   Guziewicz, M.; Grochowski, J.; Borysiewicz, M.; et al. Electrical and optical properties of NiO films deposited by magnetron sputtering. *Opt. Appl.* **2011**, *41*, 431.

3.   Xu, J.; Boyd, C.C.; Yu, Z.J.; et al. Triple-halide wide–band gap perovskites with suppressed phase segregation for efficient tandems. *Science* **2020**, *367*, 1097.

4.   Hou, Y.; Aydin, E.; De Bastiani, M.; et al. Efficient tandem solar cells with solution-processed perovskite on textured crystalline silicon. *Science* **2020**, *367*, 1135.

5.   De Bastiani, M.; Mirabelli, A.J.; Hou, Y.; et al. Efficient bifacial monolithic perovskite/silicon tandem solar cells via bandgap engineering. *Nat. Energy* **2021**, *6*, 167.

6.   Kamino, B.A.; Paviet-Salomon, B.; Moon, S.J.; et al. Low-Temperature Screen-Printed Metallization for the Scale-Up of Two-Terminal Perovskite–Silicon Tandems. *ACS Appl. Energy Mater.* **2019**, *2*, 3815.

7.   Dussouillez, M.; Moon, S.; Mensi, M.; et al. Understanding and Mitigating the Degradation of Perovskite Solar Cells Based on a Nickel Oxide Hole Transport Material during Damp Heat Testing. *ACS Appl. Mater. Interfaces* **2022**, *15*, 27941.

8.   Karsthof, R.; Anton, A.M.; Kremer, F.; et al. Nickel vacancy acceptor in nickel oxide: Doping beyond thermodynamic equilibrium. *Phys. Rev. Mater.* **2020**, *4*, 034601.

9.   Boyd, C.C.; Shallcross, R.C.; Moot, T.; et al. Overcoming Redox Reactions at Perovskite-Nickel Oxide Interfaces to Boost Voltages in Perovskite Solar Cells. *Joule* **2020**, *4*, 1759.

10. Itzhak, A.; He, X.; Kama, A.; et al. NiN-Passivated NiO Hole-Transport Layer Improves Halide Perovskite-Based Solar Cell. *ACS Appl. Mater. Interfaces* **2022**, *14*, 47587.

11. Peng, Z.; Zuo, Z.; Qi, Q.; et al. Managing the Double-Edged Sword of Ni3+ in Sputter-Deposited NiOx by Interfacial Redox Reactions for Efficient Perovskite Solar Cells. *ACS Appl. Energy Mater.* **2023**, *6*, 1396.

12. Guo, Y.; Ma, J.; Wang, H.; et al. Overcoming Ni^{3+}-Induced Non-Radiative Recombination at Perovskite-Nickel Oxide Interfaces to Boost Voltages in Perovskite Solar Cells. *Adv. Mater. Interfaces* **2021**, *8*, 1.

13. Li, C.; Wang, X.; Bi, E.; et al. Rational design of Lewis base molecules for stable and efficient inverted perovskite solar cells. *Science* **2023**, *379*, 690.

14. Zhang, C.; Shen, X.; Chen, M.; et al. Constructing a Stable and Efficient Buried Heterojunction via Halogen Bonding for Inverted Perovskite Solar Cells. *Adv. Energy Mater.* **2023**, *13*, 2203250.

15. Lee, S.; Lee, J.; Park, H.; et al. Defect-Passivating Organic/Inorganic Bicomponent Hole-Transport Layer for High Efficiency Metal-Halide Perovskite Device. *ACS Appl. Mater. Interfaces* **2020**, *12*, 40310.

16. Phung, N.; Verheijen, M.; Todinova, A.; et al. Enhanced Self-Assembled Monolayer Surface Coverage by ALD NiO in p-i-n Perovskite Solar Cells. *ACS Appl. Mater. Interfaces* **2022**, *14*, 2166.

17. Yu, X.; Wang, Y.; Li, L.; et al. Interfacial modification of NiOx by self-assembled monolayer for efficient and stable inverted perovskite solar cells. *Chin. J. Chem. Phys.* **2024**, 37, 553.

18. Alghamdi, A.R.M.; Yanagida, M.; Shirai, Y.; et al. Surface Passivation of Sputtered NiOx Using a SAM Interface Layer to Enhance the Performance of Perovskite Solar Cells. *ACS Omega* **2022**, *7*, 12147.

19. Yan, X.; Zheng, J.; Zheng, L.L.; et al. Optimization of sputtering NiO*x* films for perovskite solar cell applications. *Mater. Res. Bull.* **2018**, *103*, 150.

20. Shi, J.; Lai, L.; Zhang, P.; et al. Aluminum doped nickel oxide thin film with improved electrochromic performance from layered double hydroxides precursor in situ pyrolytic route. *J. Solid State Chem.* **2016**, *241*, 1.

21. Chen, W.; Liu, F.Z.; Feng, X.Y.; et al. Cesium Doped NiO*x* as an Efficient Hole Extraction Layer for Inverted Planar Perovskite Solar Cells. *Adv. Energy Mater.* **2017**, *7*, 1700722.

22. Li, G.; Jiang, Y.; Deng, S.; et al. Overcoming the Limitations of Sputtered Nickel Oxide for High-Efficiency and Large-Area Perovskite Solar Cells. *Adv. Sci.* **2017**, *4*, 1700463.

23. Yao, Q.; Zhao, L.; Sun, X.; et al. Na2S decorated NiOx as effective hole transport layer for inverted planar perovskite solar cells. *Mater. Sci. Semicond. Process* **2023**, *153*, 107107.

24. Chen, W.; Wu, Y.; Yue, Y.; et al. Efficient and stable large-area perovskite solar cells with inorganic charge extraction layers. *Science* **2015**, *350*, 944.

25. Traore, B.; Pedesseau, L.; Blancon, J.C.; et al. Importance of Vacancies and Doping in the Hole-Transporting Nickel Oxide Interface with Halide Perovskites. *ACS Appl. Mater. Interfaces* **2020**, *12*, 6633.

26. Niu, G.; Wang, S.; Li, J.; et al. Oxygen doping in nickel oxide for highly efficient planar perovskite solar cells. *J. Mater. Chem. A Mater.* **2018**, *6*, 4721.

27.	Biesinger, M.C.; Payne, B.P.; Lau, L.W.M.; et al. X-ray photoelectron spectroscopic chemical state quantification of mixed nickel metal, oxide and hydroxide systems. *Surf. Interface Anal.* **2009**, *41*, 324.

28.	Biesinger, M.C.; Payne, B.P.; Grosvenor, A.P.; et al. Resolving surface chemical states in XPS analysis of first row transition metals, oxides and hydroxides: Cr, Mn, Fe, Co and Ni. *Appl. Surf. Sci.* **2011**, *257*, 2717.

29.	Islam, M.B.; Yanagida, M.; Shirai, Y.; et al. NiOx Hole Transport Layer for Perovskite Solar Cells with Improved Stability and Reproducibility. *ACS Omega* **2017**, *2*, 2291.

30.	Predanocy, M.; Hotový, I.; Čaplovičová, M. Structural, optical and electrical properties of sputtered NiO thin films for gas detection. *Appl. Surf. Sci.* **2017**, *395*, 208.

31.	Islam, R.; Chen, G.; Ramesh, P.; et al. Investigation of the Changes in Electronic Properties of Nickel Oxide (NiOx) Due to UV/Ozone Treatment. *ACS Appl. Mater. Interfaces* **2017**, *9*, 17201.

32.	Fu, F.; Pisoni, S.; Jeangros, Q.; et al. I2 vapor-induced degradation of formamidinium lead iodide based perovskite solar cells under heat–light soaking conditions. *Energy Environ. Sci.* **2019**, *12*, 3074.

33.	Shannon, R.D. Revised effective ionic radii and systematic studies of interatomic distances in halides and chalcogenides. *Acta Crystallogr. Sect. A* **1976**, *32*, 751.

34.	Bakar, W.A.W.A.; Othman, M.Y.; Ali, R.; et al. The Investigation of Active Sites on Nickel Oxide Base Catalysts towards the In-situ Reactions of Methanation and Desulfurization. *Mod. Appl. Sci.* **2009**, *3*, 35.

35.	Uhlenbrock, S.; Scharfschwerdt, C.; Neumann, M.; et al. The influence of defects on the Ni 2p and O 1s XPS of NiO. *J. Phys. Condens. Matter* **1992**, *4*, 7973.